Energy & Environmental Science

COMMUNICATION

View Article Online
View Journal | View Issue

Cite this: *Energy Environ. Sci.*, 2016, **9**, 2020

Received 8th April 2016,
Accepted 18th April 2016

DOI: 10.1039/c6ee01046f

www.rsc.org/ees

An efficient bifunctional two-component catalyst for oxygen reduction and oxygen evolution in reversible fuel cells, electrolyzers and rechargeable air electrodes†

Sören Dresp, Fang Luo, Roman Schmack, Stefanie Kühl, Manuel Gliech and Peter Strasser*

We report on a non-precious, two-phase bifunctional oxygen reduction and evolution (ORR and OER) electrocatalyst with previously unachieved combined roundtrip catalytic reactivity and stability for use in oxygen electrodes of unitized reversible fuel cell/electrolyzers or rechargeable metal–air batteries. The combined OER and ORR overpotential, total, at 10 mA cm^{-2} was a record low value of 0.747 V. Rotating Ring Disk Electrode (RRDE) measurements revealed a high faradaic selectivity for the 4 electron pathways, while subsequent continuous MEA tests in reversible electrolyzer cells confirmed the excellent catalyst reactivity rivaling the state-of-the-art combination of iridium (OER) and platinum (ORR).

Broader context

The transformation of our existing fossil fuel-based energy systems into renewable fuel-based ones will require advances and innovations from chemistry and catalysis science. In particular, efficient, low cost and abundant catalysts for the two-way conversion of electricity into, as well as the generation of electricity from high-energy molecules, such as molecular hydrogen, will be critical. "One way" hydrogen-based devices that facilitate these chemical processes, such as fuel cells and electrolyzers, typically depend on catalyst materials that are high in price and low in abundance, like platinum and iridium oxide. Earth-abundant bifunctional catalysts, on the other hand, that can act as "two-way" catalysts and combine the fuel cell as well as the electrolyzer functions would allow the design of compact (reversible) unitized regenerative fuel cells (URFC). Here, we report on a facile design concept, and the synthesis, activity, selectivity and device performance of bifunctional oxygen electrode (oxygen reduction and oxygen evolution) catalysts. Deployed in gas diffusion electrodes, our heterogeneous two-component catalysts display previously unachieved bifunctional catalytic activity.

Electrochemical energy storage based on the interconversion of renewable electricity and molecular fuels (solar fuels) and solid state structures (aqueous metal–air cells) invariably involves the oxygen/water redox system supplying and consuming water, protons, electrons and oxygen. This is why efficient catalysts for the oxygen evolution reaction (OER: $4OH^- \rightarrow O_2 + 2H_2O + 4e^-$) and the oxygen reduction reaction (ORR: $O_2 + 2H_2O + 4e^- \rightarrow 4OH^-$) are critical.[1–4] Combining the two functionalities in one single bifunctional oxygen redox electrode would greatly simplify the design of energy conversion devices or enhance the mobility and power-to-weight ratio. This plays an important role in spacecraft, aircraft, and ground transportation applications. Active oxygen redox catalysts such as IrO_2 or Pt are rare and expensive, which is why the development of efficient non-precious oxygen catalysts is of interest.[5–10] The layered double hydroxide of Ni and Fe ("NiFe-LDH") is known to be one of the most active non-noble OER catalysts in alkaline solution.[5,11–26] In contrast, nitrogen-doped carbon materials are promising non-precious candidates for the ORR.[27–30] Rather than exploring suitable bifunctional catalytic surface sites, or designing two distinct active sites on the same substrate, we propose the facile heterogeneous mixing of either material to obtain a two-phase bifunctional catalyst. This was shown for noble metal catalysts of iridium and platinum.[31,32] Recently, non-precious metal mixtures of Mn–Co oxides and carbon nanotubes have been tested.[33] Realizing that a two-component surface is necessary for highly active bifunctional catalysts,[34,35] in this contribution, we designed two-component NiFe-LDH – Fe–N–C catalysts resulting in today's most efficient bifunctional oxygen electrodes in 0.1 M KOH. A mutual improving effect between the two components in the two-phase structure with distinct neighbouring active sites appears key to the observed performance.

Using a fast microwave-assisted solvothermal one-pot synthesis route (Fig. S1, ESI†), we prepared a carbon-supported crystalline NiFe-LDH catalyst material in a Ni/Fe ratio of ~3.6 ($Ni_{0.78}Fe_{0.22}(OH)_x$) and a metal loading of ~37 wt%. The X-ray diffraction (XRD) pattern (Fig. 1) is consistent with the data-based reflections of layered double hydroxides (JCPDS: 00-014-0191), but with slightly higher interlayer distances.[36]

TEM images of NiFe-LDH/C show very small (~2–4 nm) plates presumably representing NiFe-LDH flakes. SAED revealed instability of the LDH phase under TEM working conditions

Department of Chemistry, Technical University Berlin, 10623 Berlin, Germany

† Electronic supplementary information (ESI) available. See DOI: 10.1039/c6ee01046f

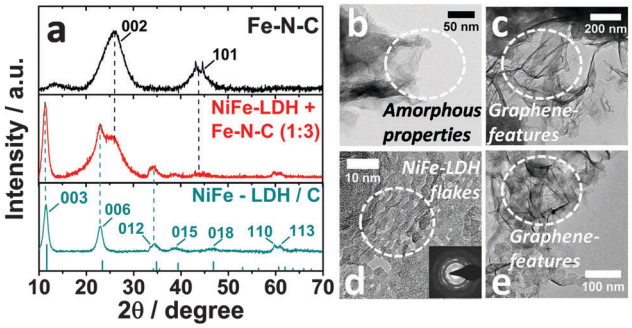

Fig. 1 (a) X-ray diffraction profiles of the Fe N-doped carbon catalyst (Fe–N–C) (top), the mixture of NiFe-LDH and Fe–N–C catalysts (middle) and the carbon-supported NiFe-layered double hydroxide catalyst (NiFe-LDH/C) in an atomic ratio of ~3.6 ($Ni_{0.78}Fe_{0.22}(OH)_x$) (bottom); (b and c) TEM images of Fe–N–C; and (d and e) TEM images of NiFe-LDH/C.

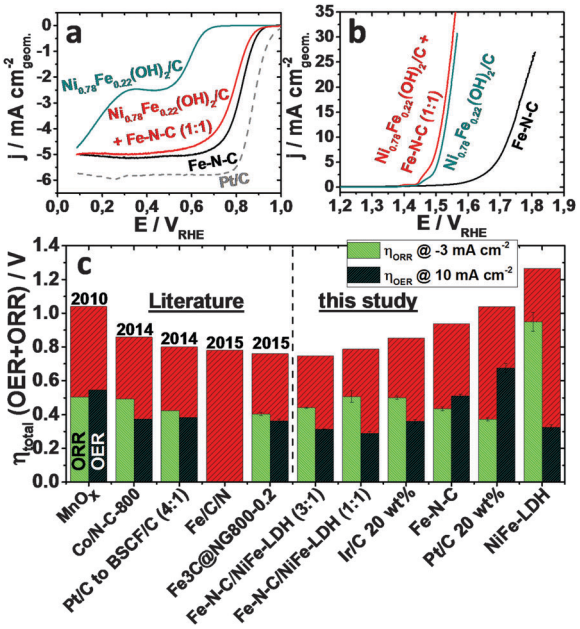

Fig. 2 Catalytic ORR (a) and OER (b) voltammetric profile and activity of the pure NiFe-LDH, pure Fe–N–C catalysts, and of their two-component mixture in O_2-saturated 0.1 M KOH at 5 mV s^{-1} scan rate, 1600 rpm rotation speed and 0.2 mg cm^{-2} total catalyst loading; and (c) individual ORR and OER, and total overpotentials for six different catalysts of this study (right side) in comparison to the published literature (left side). Fe–N–C/NiFe-LDH (*X* : *Y*) denote novel two-phase catalysts reported here. Detailed activity values are given in Table S1 (ESI†).

(high vacuum and e^--beam) since only NiO (JCPDS: 03-065-2901), possibly mixed with FeO (JCPDS: 01-077-2355), was detected. Furthermore, NiFe-LDH/C showed graphene features as shown in Fig. 1e which evolved from the carbon black support. The Fe–N–C material was synthesized using aniline polymerization in the presence of $FeCl_3$, followed by repetitive annealing and acid leaching to dissolve the residual Fe species, which may block the active sites in the catalyst material (see the ESI† and Fig. S2).[37] The XRD pattern showed largely graphene reflections (JCPDS: 98-000-0231) (Fig. 1a). In fact, the graphene morphology is detected by TEM (Fig. 1c). Additional TEM images suggest a strong amorphization of the remaining sample (Fig. 1b), which is in accordance with the XRD data due to non-appearance of strong reflections. When we mixed the samples, the XRD data reveal a two-phase system with reflections of both samples. So we believe that the catalyst system is a mixed two component system with separated phases. Supporting this, TEM images show graphene features as well as a flake like structure almost similar to the features of each of the other samples (Fig. S8, ESI†).

Electrochemical activity

First, we investigated the OER and ORR activity in O_2-saturated 0.1 M KOH at 1600 rpm separately for both catalysts. The results are shown in Fig. 2a and b. Linear sweep voltammetry verified the high OER activity for NiFe-LDH/C and high ORR activity for the Fe–N–C material. As expected, either material showed essentially no activity for the reverse reactions: NiFe-LDH was almost inactive for ORR and Fe–N–C for OER.

We then tested a two-component mixture of the catalysts keeping the total catalyst loading at 0.2 mg cm^{-2} in all measurements. Our data showed that all the beneficial features of NiFe-LDH and Fe–N–C are fully unfolded in the mixture due to the presence of the other component.

Fig. 2b demonstrates that the two-phase Fe–N–C/NiFe-LDH (1 : 1) sample showed a slightly higher OER activity than the identical NiFe-LDH alone. This could be due to a higher surface area or improved conductivity indicated by a higher $Ni^{2+/3+}$ redox peak[11,13,23,38] presented in Fig. S9 (ESI†), which is also indicated by capacitive measurements in N_2 presented in Fig. S10 (ESI†). We further note that the ORR activity of the two-phase powder catalyst, at constant OER activity, could be significantly increased by increasing the Fe–N–C/NiFe-LDH ratio to 3 : 1 (see "Fe–N–C/NiFe-LDH (3 : 1)" catalyst).

Fig. 2c shows the combined overpotentials, $\eta_{total} = \eta_{OER} + \eta_{ORR}$, of our two-phase catalysts and some previously reported materials in a reversible oxygen electrode. The parameter η_{total} describes the effective combined oxygen overpotential of the OER overpotential at 10 mA cm^{-2} and the half-wave ORR potential ($E_{1/2}$) at −3 mA cm^{-2} and 1600 rpm.[39,40] The evolution of reported η_{total} values (Fig. 2c left) compared to those of the present study (Fig. 2c right) demonstrates the superiority of our two-phase catalysts. While in 2010 a single-phase Mn-oxide based catalyst has been shown to have an overpotential of η_{total} = 1.04 V, our Fe–N–C/NiFe-LDH (3 : 1) catalyst reached the value of 0.747 V ± 0.006 V and thus represents the most efficient bifunctional oxygen redox RDE activity to date. It should be mentioned that in 2011 Liang *et al.* prepared Co_3O_4 on N-doped graphene with a lower total overpotential of $\Delta\eta_{total}$ = 0.71 V, this however in 1 M KOH, not 0.1 M KOH.[41] In addition, our material has outstanding individual OER activity with an overpotential of 0.309 ± 0.002 V *vs.* RHE at 10 mA cm^{-2}. This is a lower overpotential than that of IrO_2 and is one of the best bifunctional catalysts in 0.1 M KOH (Fig. 2c, details in Table S1, ESI†). To explain the observed combined performance of a physical mixture, our preliminary studies confirm[34,35] that a

simple two-phase system provides two distinct and spatially separated ORR and OER catalytic sites that are sufficiently homogeneous to act as a contiguous catalyst film, yet are spatially separated enough not to interfere with each other. Based on our available data, we cannot exclude the formation of special 3D structured active sites by physical atomic proximity of OER and ORR sites on either component, as suggested by Rossmeisl and co-workers to overcome restrictive adsorption scaling relations.[42–44] Following this track, the combination of two active sites for the generation of a multisurface site was also suggested by Norskov *et al.* as a new design paradigm for heterogeneous catalysts.[45]

Selectivity

Rotating ring disk electrode (RRDE) measurements were carried out to determine the ORR selectivities under alkaline conditions (Fig. 3a). The ORR reaction diagram (Fig. 3b[46–48]) highlights the direct 4e$^-$ pathway to OH$^-$ and the 2e$^-$ pathway to HO_2^- which may desorb into the solution, subsequently react in a 2e$^-$ process to OH$^-$, or else undergo chemical disproportionation. The ring potential was kept at +1.2 V_{RHE} to monitor the desorbed HO_2^- species upon its re-oxidation to oxygen at the ring (see Fig. 3c). Almost similar to Fe–N–C the RRDE data revealed a high selectivity (>90% at $E > 0.2$ V) towards the direct 4-electron pathway to OH$^-$ for the Fe–N–C/NiFe-LDH (3 : 1) catalyst, compared to glassy carbon (12–17%) or the 20 wt% Pt/C reference (86%). A completely different behaviour of NiFe-LDH that showed a strong increase of H_2O_2 production at low overpotentials was observed. After passing a maximum of ~76% at 0.45 V *vs.* RHE, the production rate of H_2O_2 drops and the kinetics change to a 4e$^-$ transfer reaction to OH$^-$ at 0.1 V *vs.* RHE. Evaluation of the number of transferred electrons during the reaction further revealed an almost ideal 4-electron transfer over the full potential range for all Fe–N–C based catalysts (Fig. 3d). Furthermore, we confirmed O_2 production during OER for NiFe-LDH *via* RRDE measurements as presented in the ESI,† Fig. S11. Therefore we kept the potential at 0.31 V *vs.* RHE to reduce the oxygen to HO_2^-. We further determined an efficiency of almost 100% at 1.5 V *vs.* RHE. At higher potentials the faradaic efficiency drops, which can be explained by mass transfer limitations of the gaseous oxygen produced at the disk.

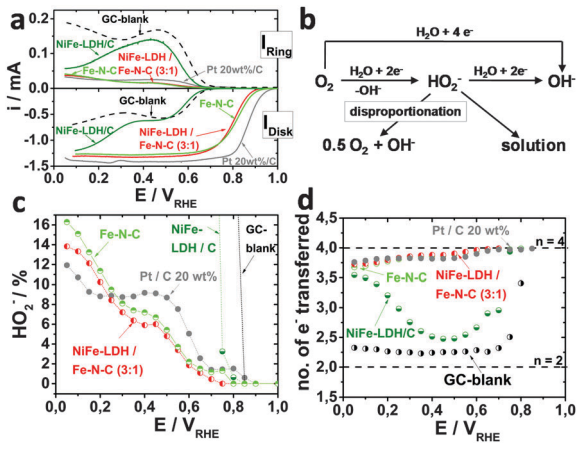

Fig. 3 (a) Rotating Ring Disk Electrode (RRDE) selectivity measurements; (b) reaction pathways of the ORR; (c) faradaic HO_2^- selectivities of Fe–N–C (green), Fe–N–C/NiFe-LDH (3 : 1) (red), Pt (grey), and carbon (dashed line,); and (d) the number of transferred electrons as a function of electrode potential.

Unitized fuel cell/electrolyzer performance

Unitized alkaline exchange membrane-based single-cell fuel cell/electrolyzer measurements were carried out to study the catalyst performance under real conditions (Fig. 4a). Alternating fuel cell/electrolyzer polarization tests revealed an unprecedented activity for the noble metal-free Fe–N–C/NiFe-LDH (3 : 1) positive electrode material rivaling the Ir catalyst. Platinum, as expected, showed excellent fuel cell but poor electrolyzer performance (Fig. 4b).

In Fig. 4c a cell stability test is presented for the Fe–N–C/NiFe-LDH (3 : 1) catalyst, where the polarization curves were recorded in alternating fuel cell and electrolyzer modes. The fuel cell activity decreased gradually after each cycle. The initial round trip efficiency (RTE) decreased from 50% to 45% in the second cycle. This was superior to the performance of the two noble-metal reference catalysts (Fig. S14, ESI†), indicating a higher reversibility of the bifunctional two-component catalyst.

To evaluate stability we conducted a long term RDE measurement. Fig. 4d presents a 24 h galvanostatic RDE stability test of the Fe–N–C/NiFe-LDH (3 : 1) catalyst. Currents were held for 1 h, alternating between the fuel cell and electrolyzer modes.

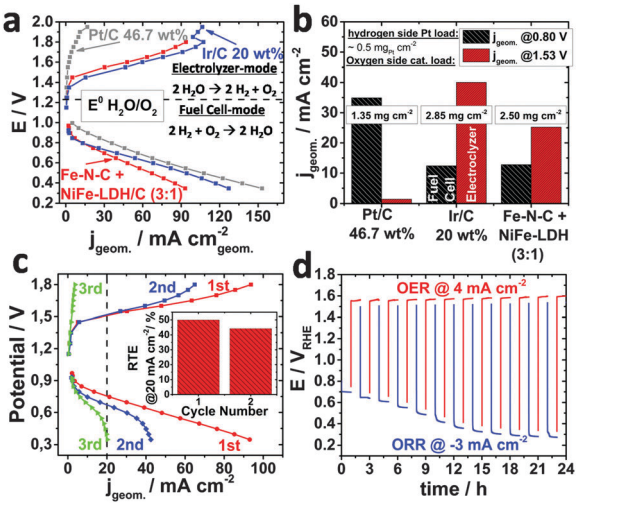

Fig. 4 Full alkaline exchange membrane (AEM)-based unitized MEA fuel/electrolysis cell measurements: (a) polarization curves for the first fuel cell/electrolysis cycle with platinum as the hydrogen catalyst, and platinum (grey), iridium (blue) and the Fe–N–C/NiFe-LDH (3 : 1) as the oxygen catalysts. (b) Comparison of geometric activities of the three unitized cells. (c) Three consecutive fuel cell/electrolyzer cycles using the Fe–N–C/NiFe-LDH (3 : 1) catalyst, inset: round trip efficiency (RTE) for the first two cycles. (d) 24 h RDE stability measurement of unitized fuel/electrolysis cell using the Fe–N–C/NiFe-LDH (3 : 1) catalyst. Unitized fuel cell/electrolyzer performance.

To reduce bubble formation the OER current was held at 4 mA cm^{-2} and the ORR current was held at −3 mA cm^{-2}, which represents approximately the half wave potential ($E_{1/2}$) at 1600 rpm.

Clearly, the OER cell potentials remained constant and stable for the entire 24 h test highlighting the stability of the NiFe-LDH OER system. The slightly larger performance drop in fuel cell mode is consistent with the data from Fig. 4c and the RDE data. The oxygen reduction potential decreased per each OER/ORR cycle until it remained constant at approximately 0.3 V. We attribute this to the electrochemical oxidation of the active Fe–N–C sites combined with electrochemical carbon corrosion which is also indicated by the strong activity decrease during OER for the Fe–N–C catalyst presented in Fig. S13 (ESI†).[49] We believe that stronger graphitization at a higher temperature could prevent the strong degradation of this material. Further TEM and SEAD measurements of the two-component system indicated beside a strong agglomeration an increased crystallinity and nanoparticle formation after the electrochemical treatment (Fig. S8, ESI†).

In conclusion, we present a microwave-assisted synthesis of highly OER active NiFe-LDH. Physical mixing with a Fe–N–C catalyst in a highly active bifunctional oxygen electrode catalyst for use at unitized oxygen electrodes. This catalyst exhibited the lowest combined OER/ORR overpotential ever recorded in 0.1 M KOH. RRDE investigation showed high ORR selectivity. Beyond RDE screenings, we further reported anion exchange membrane electrode assembly tests (AEM-MEA) in a reversible electrolyzer. The non-noble mixture catalysts outperformed Pt and rivaled Ir reference catalysts. During alternating electrolyzer and fuel cell tests the ORR cell performance revealed a larger degradation compared to the OER cell performance, suggesting that the OER potentials damage the carbon-based Fe–N–C ORR active sites, which might be improved by stronger graphitization using a higher annealing temperature or replacing the graphitic Fe–N–C catalyst by Fe–N doped graphene.

Acknowledgements

Financial support by the German Research Foundation (DFG) through grant reference number STR 596/8-1 and the Federal Ministry of Education and Research (BMBF) grant 03SF0433A ''MEOKATS'' are grateful acknowledged. S. K. acknowledges financial support under BMBF grant 03SF0527A ''LOPLAKAT''. Also, we acknowledge the ZELMI for making the TEM micrograph.

Notes and references

1 L. Barreto, A. Makihira and K. Riahi, *Int. J. Hydrogen Energy*, 2003, **28**, 267–284.
2 S. M. Fernández Valverde, *Geofis. Int.*, 2002, **41**, 223–228.
3 G. Marbán and T. Valdés-Solís, *Int. J. Hydrogen Energy*, 2007, **32**, 1625–1637.
4 R. Schlogl, *ChemSusChem*, 2010, **3**, 209–222.
5 C. C. L. McCrory, S. Jung, J. C. Peters and T. F. Jaramillo, *J. Am. Chem. Soc.*, 2013, **135**, 16977–16987.
6 H. A. Gasteiger, S. S. Kocha, B. Sompalli and F. T. Wagner, *Appl. Catal., B*, 2005, **56**, 9–35.
7 M. Heggen, M. Oezaslan, L. Houben and P. Strasser, *J. Phys. Chem. C*, 2012, **116**, 19073–19083.
8 R. Forgie, G. Bugosh, K. C. Neyerlin, Z. C. Liu and P. Strasser, *Electrochem. Solid-State Lett.*, 2010, **13**, D36–D39.
9 E. Ortel, T. Reier, P. Strasser and R. Kraehnert, *Chem. Mater.*, 2011, **23**, 3201–3209.
10 M. Oezaslan, F. Hasche and P. Strasser, *J. Electrochem. Soc.*, 2012, **159**, B394–B405.
11 L. Trotochaud, S. L. Young, J. K. Ranney and S. W. Boettcher, *J. Am. Chem. Soc.*, 2014, **136**, 6744–6753.
12 M. W. Louie and A. T. Bell, *J. Am. Chem. Soc.*, 2013, **135**, 12329–12337.
13 L. Trotochaud, J. K. Ranney, K. N. Williams and S. W. Boettcher, *J. Am. Chem. Soc.*, 2012, **134**, 17253–17261.
14 D. A. Corrigan, *J. Electrochem. Soc.*, 1987, **134**, 377–384.
15 D. A. Corrigan, R. S. Conell, C. A. Fierro and D. A. Scherson, *J. Phys. Chem.*, 1987, **91**, 5009–5011.
16 R. L. Doyle, I. J. Godwin, M. P. Brandon and M. E. G. Lyons, *Phys. Chem. Chem. Phys.*, 2013, **15**, 13737–13783.
17 C.-C. Hu and Y.-R. Wu, *Mater. Chem. Phys.*, 2003, **82**, 588–596.
18 M. E. G. Lyons and M. P. Brandon, *Int. J. Electrochem. Sci.*, 2008, **3**, 1386–1424.
19 C. C. L. McCrory, S. Jung, I. M. Ferrer, S. M. Chatman, J. C. Peters and T. F. Jaramillo, *J. Am. Chem. Soc.*, 2015, **137**, 4347–4357.
20 M. D. Merrill and R. C. Dougherty, *J. Phys. Chem. C*, 2008, **112**, 3655–3666.
21 E. L. Miller and R. E. Rocheleau, *J. Electrochem. Soc.*, 1997, **144**, 3072–3077.
22 E. Potvin and L. Brossard, *Mater. Chem. Phys.*, 1992, **31**, 311–318.
23 X. Yu, M. Zhang, W. Yuan and G. Shi, *J. Mater. Chem. A*, 2015, **3**, 6921–6928.
24 K. Zeng and D. Zhang, *Prog. Energy Combust. Sci.*, 2010, **36**, 307–326.
25 F. Dionigi, T. Reier, Z. Pawolek, M. Gliech and P. Strasser, *ChemSusChem*, 2016, DOI: 10.1002/cssc.201501581.
26 M. Görlin, P. Chernev, J. Ferreira de Araújo, T. Reier, S. Dresp, B. Paul, R. Krähnert, H. Dau and P. Strasser, *J. Am. Chem. Soc.*, 2016, DOI: 10.1021/jacs.6b00332.
27 G. Wu, K. L. More, C. M. Johnston and P. Zelenay, *Science*, 2011, **332**, 443–447.
28 D. Geng, Y. Chen, Y. Chen, Y. Li, R. Li, X. Sun, S. Ye and S. Knights, *Energy Environ. Sci.*, 2011, **4**, 760–764.
29 W. Li, J. Wu, D. C. Higgins, J.-Y. Choi and Z. Chen, *ACS Catal.*, 2012, **2**, 2761–2768.
30 L. Lin, Q. Zhu and A.-W. Xu, *J. Am. Chem. Soc.*, 2014, **136**, 11027–11033.
31 S. Zhigang, Y. Baolian and H. Ming, *J. Power Sources*, 1999, **79**, 82–85.
32 S.-Y. Huang, P. Ganesan, H.-Y. Jung and B. N. Popov, *J. Power Sources*, 2012, **198**, 23–29.
33 A. Zhao, J. Masa, W. Xia, A. Maljusch, M.-G. Willinger, G. Clavel, K. Xie, R. Schlögl, W. Schuhmann and M. Muhler, *J. Am. Chem. Soc.*, 2014, **136**, 7551–7554.

34 M. Risch, K. A. Stoerzinger, S. Maruyama, W. T. Hong, I. Takeuchi and Y. Shao-Horn, *J. Am. Chem. Soc.*, 2014, **136**, 5229–5232.
35 W. T. Hong, M. Risch, K. A. Stoerzinger, A. Grimaud, J. Suntivich and Y. Shao-Horn, *Energy Environ. Sci.*, 2015, **8**, 1404–1427.
36 M. Gabrovska, D. Crisan, N. Stanica, D. Nikolova, L. Bilyarska, M. Crisan and R. Edreva-Kardjieva, *Rev. Roum. Chim.*, 2014, **59**, 447–452.
37 N. R. Sahraie, J. P. Paraknowitsch, C. Göbel, A. Thomas and P. Strasser, *J. Am. Chem. Soc.*, 2014, **136**, 14486–14497.
38 M. Gong, Y. Li, H. Wang, Y. Liang, J. Z. Wu, J. Zhou, J. Wang, T. Regier, F. Wei and H. Dai, *J. Am. Chem. Soc.*, 2013, **135**, 8452–8455.
39 Y. Zhao, K. Kamiya, K. Hashimoto and S. Nakanishi, *J. Phys. Chem. C*, 2015, **119**, 2583–2588.
40 Y. Gorlin and T. F. Jaramillo, *J. Am. Chem. Soc.*, 2010, **132**, 13612–13614.
41 Y. Liang, Y. Li, H. Wang, J. Zhou, J. Wang, T. Regier and H. Dai, *Nat. Mater.*, 2011, **10**, 780–786.
42 N. B. Halck, V. Petrykin, P. Krtil and J. Rossmeisl, *Phys. Chem. Chem. Phys.*, 2014, **16**, 13682–13688.
43 R. Frydendal, M. Busch, N. B. Halck, E. A. Paoli, P. Krtil, I. Chorkendorff and J. Rossmeisl, *ChemCatChem*, 2015, **7**, 149–154.
44 I. C. Man, H. Y. Su, F. Calle-Vallejo, H. A. Hansen, J. I. Martinez, N. G. Inoglu, J. Kitchin, T. F. Jaramillo, J. K. Norskov and J. Rossmeisl, *ChemCatChem*, 2011, **3**, 1159–1165.
45 A. Vojvodic and J. K. Nørskov, *National Science Review*, 2015, **2**, 140–149.
46 N. S. Georgescu, A. J. J. Jebaraj and D. Scherson, *ECS Electrochem. Lett.*, 2015, **4**, F39–F42.
47 C. F. Zinola, A. M. Castro Luna, W. E. Triaca and A. J. Arvia, *J. Appl. Electrochem.*, 1994, **24**, 531–541.
48 Y. Gorlin, C.-J. Chung, D. Nordlund, B. M. Clemens and T. F. Jaramillo, *ACS Catal.*, 2012, **2**, 2687–2694.
49 K. G. Gallagher, R. M. Darling and T. F. Fuller, *Handbook of Fuel Cells*, John Wiley & Sons, Ltd, 2010.

